RCFA for Recurring Impeller Failures in a 4.7 Mtpa
LNG Train Propane Compressor

Nicholas White
Machinery & Reliability Advisor
RasGas Company
Ras Laffan, Qatar

Scot Laney
Materials Engineer
Elliott Group
Jeannette, Pa, USA

Cory Zorzi
Technical Improvement Leader
Elliott Group
Jeannette, Pa, USA

Nicholas White is the Machinery and Reliability Advisor with RasGas, Qatar. His responsibilities include asset rotating machinery surveillance, trouble shooting and reliability improvement. He has previously held senior engineering positions in turbomachinery design for Alstom Power and Kellogg Brown and Root during his 12 year career.

Dr. White received his BEng (1997) and PhD (2003) degrees from the Universities of Leicester and Cranfield, UK in mechanical engineering and turbomachinery aero-thermal design. He is a chartered member of the Institution of Mechanical Engineers, UK.

Scot Laney is a Materials Engineer with the Elliott Group, in Jeannette, Pennsylvania. He joined Elliott in 2007 and has been involved with materials related R&D projects, failure analysis and aftermarket support. He also has experience in the areas of high temperature oxidation/corrosion and protective coatings.

Dr. Laney received his BS (2001), MS (2004), and PhD (2007) degrees from the University of Pittsburgh in materials science and engineering. He is also a member of ASM.

Cory Zorzi is a Mechanical Engineer for the Elliott Group in Jeannette, Pennsylvania. Mr. Zorzi has been employed with the Elliott Group since 2007 and is currently working in Research and Development. His responsibilities include root cause analysis and permanent corrective action implementation pertaining to field equipment issues.

Mr. Zorzi has a B.S. degree from The University of Pittsburgh (2006) and an MBA from Seton Hill University (2009).

ABSTRACT

A Root Cause Failure Analysis (RCFA) for repeated impeller blade failures in a five stage centrifugal propane compressor is described. The initial failure occurred in June 2007 with a large crack found in one blade on the third impeller and two large pieces released from adjacent blades on the fourth impeller. An RCFA was performed to determine the cause of the failures. The failure mechanism was identified to be high cycle fatigue. Several potential causes related to the design, manufacture, and operation of the compressor were examined. The RCFA concluded that the design and manufacture were sound and there were no conclusive issues with respect to operation. A specific root cause was not identified. In June 2009, a second case of blade cracking occurred with a piece once again released from a single blade on the fourth impeller. Due to the commonality with the previous instance this was identified as a repeat failure. Specifically, both cases had occurred in the same compressor whereas, two compressors operating in identical service in

adjacent Liquefied natural Gas (LNG) trains had not encountered the problem. A second RCFA was accordingly launched with the ultimate objective of preventing further repeated failures.

Both RCFA teams were established comprising of engineers from the End User (RasGas), the OEM (Elliott Group) and an independent consultancy (Southwest Research Institute). The scope of the current investigation included a detailed metallurgical assessment, impeller modal frequency assessment, steady and unsteady computational fluid dynamics (CFD) assessment, finite element analyses (FEA), fluid structure interaction (FSI) assessment, operating history assessment and a comparison change analysis. By the process of elimination, the most probable causes were found to be associated with:

- vane wake excitation of either the impeller blade leading edge modal frequency from severe mistuning and/or unusual response of the 1-diameter cover/blades modal frequency
- mist carry over from third side load upstream scrubber
- end of curve operation in the compressor rear section

INTRODUCTION

RasGas currently operates seven LNG trains at Ras Laffan Industrial City, Qatar. Train 3 was commissioned in 2004 with a nameplate LNG production of 4.7 Mtpa which corresponds to a wet sour gas feed of 790 MMscfd (22.37 MMscmd). Trains 4 and 5 were later commissioned in 2005 and 2006 respectively. They were also designed for a production 4.7 Mtpa LNG but have higher wet sour gas feed rates of 850 MMscfd (24.05 MMscmd). Despite these differences, the rated operation of the propane compressor is identical in each train.
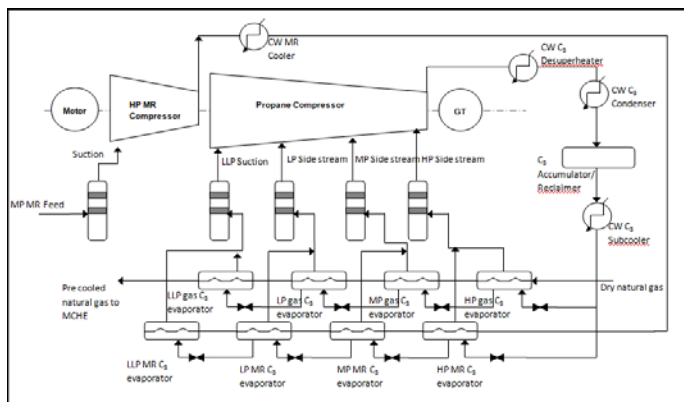

Figure 1. APCI C3-MR Refrigeration system for Trains 3, 4 and 5

The APCI C_3-MR refrigeration cycle (Roberts, et al. 2002), depicted in Figure 1 is common for all three trains. Propane is circulated in a continuous loop between four compressor inlets and a single discharge. The compressed discharge gas is cooled and condensed in three sea water cooled heat exchangers before being routed to the LLP, LP, MP and HP evaporators. Here, the liquid propane is evaporated by the transfer of heat from the warmer feed and MR gas streams. It finally passes through one of the four suction scrubbers before re-entering the compressor as a gas. Although not shown, each section inlet has a dedicated

anti-surge control loop from the de-superheater discharge to the suction scrubber inlet.

A cross section of the propane compressor casing and rotor is illustrated in Figure 2. It is a straight through centrifugal unit with a horizontally split casing. Five impellers are mounted upon the 21.3 ft (6.5 m) long shaft. Three side loads add gas upstream of the suction at impellers 2, 3 & 4. The impellers are of two piece construction, with each piece fabricated from AISI 4340 forgings that were heat treated such that the material has sufficient strength and toughness for operation at temperatures down to -50°F (-45.5°C). The blades are milled to the hub piece and the cover piece was welded to the blades using a robotic metal inert gas (MIG) welding process. The impellers are mounted to the shaft with an interference fit. The thrust disc is mounted to the shaft with a line on line fit and anti-rotation key. The return channel and side load inlets are all vaned to align the downstream swirl angle. The impeller diffusers are all vaneless. A summary of the relevant compressor design parameters is given in Table 1.

The complete compressor string is also depicted in Figure 1. The propane compressor is coupled directly to the HP MR compressor and driven by a GE Frame 7EA gas turbine and ABB 16086 HP (12 MW) helper motor at 3600 rpm rated shaft speed.

Table 1. Propane Compressor design parameters

	Component	Material	No of Vanes / Blades	Ratio of suction volume flow rate	Total Pressure Ratio
Section 1 (LLP)	Main Suction	ASTM A-36	14		
	Impeller # 1 (D = 50 in)	AISI4340	13	1.00	1.89
	Return Channel # 1	ASTM A-36	16		
Section 2 (LP)	Side Load # 1	ASTM A-36	14	0.69	
	Impeller # 2 (D = 49.1 in)	AISI4340	13	1.28	1.72
	Return Channel # 2	ASTM A-36	16		
Section 3 (MP)	Side Load # 2	ASTM A-36	14	0.61	
	Impeller # 3 (D = 48.9 in)	AISI4340	13	1.40	1.69
	Return Channel # 3	ASTM A-36	16		
Section 4 (HP)	Side Load # 3	ASTM A-36	14	0.35	
	Impeller # 4 (D = 48.3 in)	AISI4340	13		2.45
	Return Channel # 4	ASTM A-36	16	1.21	
	Impeller # 5 (D = 42.7 in)	AISI4340	15		

Train 3 had reached approximately 26,000 cumulative operating hours by February 2007, when the first failure was detected. A step change was observed in the measured radial vibration signal at the non-drive end journal bearing. The compressor was monitored closely until the scheduled train shutdown in June 2007. Vibrations during this time remained high but stable. Upon opening the casing, one cracked blade was found in the third impeller and two blade ruptures in the fourth impeller. A replacement of the complete rotor assembly was necessary which caused six days additional downtime, severely impacting LNG train availability.

Another vibration step change was encountered in October 2008, approximately 11,000 operating hours after the rotor replacement. Given the similarity of symptoms to those encountered prior to the 2007 failure, the compressor was closely monitored and operated until the next planned train shutdown in May 2009 with no further vibration steps. A released piece from a single ruptured blade on the fourth

impeller was discovered upon inspection of the opened compressor casing. Fortunately, the rotor involved in the 2007 failure had been repaired and was available. It was fitted immediately and the compressor was restarted without causing any additional outage time.

Immediately following the second failure, a detailed RCFA was commissioned. The primary objective of the investigation was to identify the contributing factors which led to the impeller blade cracks and ruptures. Moreover, to recommend actionable measures that would be required to avoid further similar failures.

The investigation considered a broad spectrum of initial possibilities. As such, this paper includes findings from metallurgical, modal frequency, measured performance, steady and unsteady CFD, finite element and fluid structure interaction studies. A team of fifteen engineers was formed including members from RasGas' Operational Technical Department, an independent consultant from the Southwest Research Institute (SwRI) and Elliott's Technical Service and Research and Development departments.
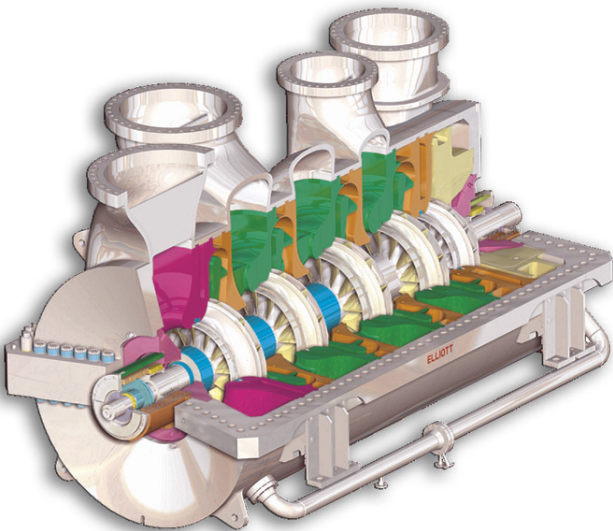

Figure 2. RasGas Train 3, 4 & 5 Propane Compressor

IMPELLER FAILURE DETECTION AND DAMAGE

A vibration step change increase from 0.63 to 1.73 mils (16 to 44 microns) was measured at the non drive end journal bearing on 8th February 2007. This remained constant until 16th April 2007, when a second step change increase to 2.52 mils (64 microns) was measured. Analysis of the vibration spectra using waterfall diagrams is shown in Figure 3. The step change occurred during steady state operation at 3600 rpm indicating a rotor unbalance increase and possible mechanical damage.

Although the vibration level was high, it remained steady and below the alarm limit of 3.15 mils (80 microns). The End User decided to accept the risk of continued operation until the next scheduled maintenance outage on 12th June 2007. At this point, the rotor had reached 29,000 operating hours. Upon inspection, one blade on the third impeller was found to have cracked and two adjacent blades on the fourth impeller had cracks with large released pieces. The fifth impeller had also

suffered blade leading edge damage from collision with the upstream released pieces. Photographs of each impeller are shown in Figures 4 – 6. The whole rotor was replaced with the warehouse spare during the scheduled shutdown. The damaged rotor was immediately packaged and shipped to the OEM for detailed inspection and repair. In total, the damaged rotor caused an additional six days of downtime, which resulted in significant losses in LNG production and revenue.
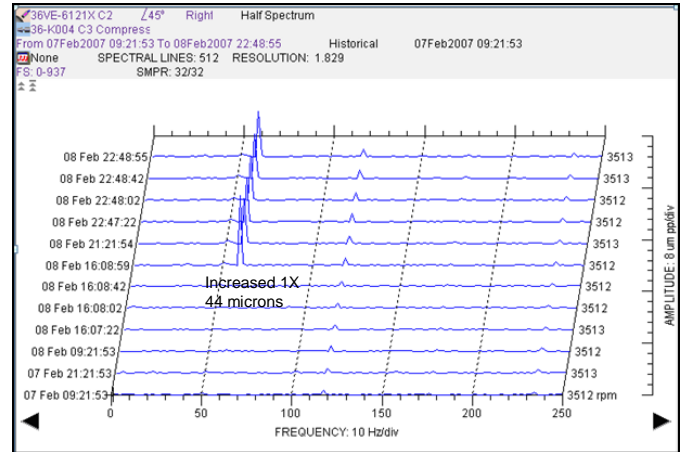
First Step Change on 8th February 2007, right half spectrum
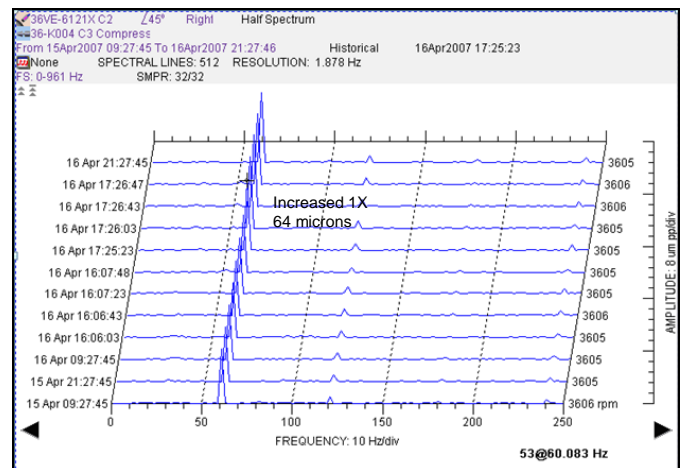
Second Step Change on 16th April 2007, right half spectrum
Figure 3. Waterfall plots for non drive end journal

On the 4th October 2008, after 11,000 operating hours, the compressor string tripped due to a process upset. Upon restart, a large vibration step change was measured at both journal bearings. The peak, from 0.63 to 4.13 mils (16 to 105 microns), was measured at the non-drive end while traversing the rotor critical speed. Based upon the previous experience from 2007, it was decided to continue operation under close surveillance until the next scheduled shutdown on 19th May 2009. It was also necessary to increase the alarm and trip limits from 3.15 and 4.13 to 6.10 and 6.49 mils (80 and 105 to 155 and 165 microns) respectively. Figure 7 shows the plotted vibration amplitudes between the 3rd and 11th October 2008 with revised alarm and trip limits. Table 2 summarizes the 1X (running frequency) vibration amplitude and the phase angle of the compressor bearings before and after the trip.
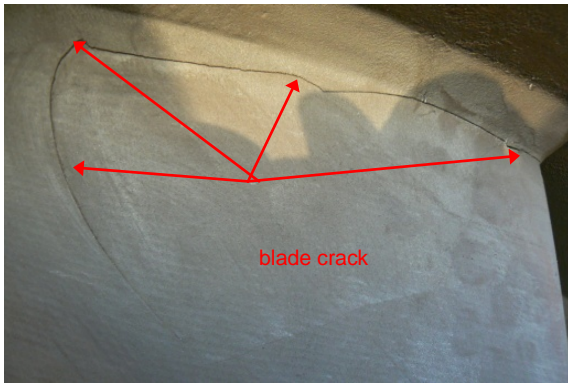
Figure 4. Third Impeller cracked blade leading edge – June 2007

Figure 5. Fourth Impeller released pieces from blade leading edge – June 2007

Figure 6. Fifth Impeller blade leading edge damage – June 2007

Table 2. Bearing vibrations before and after successful start-up

Bearing Probe Tag	Before 04 Oct 08 trip			After 05 Oct08 start up		
	Overall	1X Amp	1X Ph	Overall	1X Amp	1X Ph
36-VI6120X C1X	24 μm	16 μm	29˚	55 μm	49 μm	355˚
36-VI6120Y C1Y	21 μm	11 μm	114˚	35 μm	28 μm	94˚
36-VI6121X C2X	17 μm	2 μm	30˚	90 μm	81 μm	162˚
36-VI6121Y C2Y	16 μm	3 μm	147˚	48 μm	40 μm	259˚

The 1X vibration amplitude of the drive and non-drive end bearings (C1 and C2 respectively) increased significantly compared with those before the compressor string trip. There was a phase shift on the drive end bearing (C1X) of

approximately 30 degrees indicating a change in the rotor unbalance. The measured 1X vibrations on the non-drive end bearing before the trip were deemed too low to be reliable data. The overall and filtered 1X frequency vibrations, measured during the successful start up on 5th October 2008, indicated that the step change in the vibration amplitude was dominated by increases in the 1X running frequency component. No significant changes in the other frequency components were noted.

Inspection of the opened unit revealed that the fourth impeller had a single cracked blade with a large released piece (Figure 8). Similar to what was observed in 2007 (Figure 5), the crack appears to initiate at the leading edge of the blade close to the cover. It follows the toe of the weld before turning into the blade and returning back to the leading edge near the mid span of the blade.
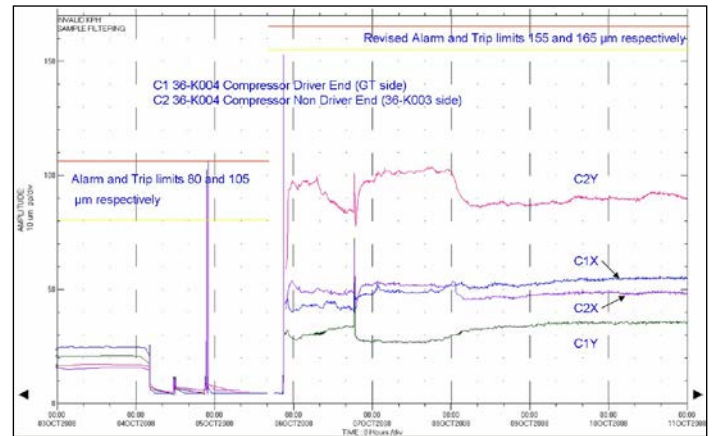

Figure 7. Bearing X and Y probe measured vibration amplitudes 3 – 11 October 2008

Figure 8. Fourth Impeller released piece at blade leading edge – June 2009

RCFA INVESTIGATIONS

An RCFA team was formed immediately following the discovery of the repeated fourth impeller failure in June 2009. Members were chosen with expertise in aero-thermodynamics, materials science, mechanical integrity, operations, process engineering and reliability engineering. A comprehensive study of the material discussed in the previous section was carried out. Moreover, the OEM members gathered references from

their experience database which had relevance to these impeller blade failures. This exercise produced the beginning hypotheses for the root cause analysis.

Four individual impeller blade failure mechanisms were postulated; material fatigue, corrosion, overload and erosion. These formed the top tier of the logic tree (Appendix A). The metallurgical analysis included a detailed inspection of the failed impellers. Evidence was found of fatigue, corrosion and erosion, but the severity of the latter two was minor. High cycle fatigue (HCF) was therefore pursued as the major failure mechanism with corrosion and erosion as possible contributing factors. The HCF branch was expanded to yield a total of 12 hypotheses for root causes. The metallurgical report showed no manufacturing defects at the initiation sites (Figure 9), which eliminated five hypotheses. Three others were eliminated by CFD analysis. Of the remaining hypotheses, three root causes were verified with varying degrees of confidence (where; 5 = true; 4 = highly likely; 3 = likely; 2 = possibly true; 1 = unlikely; 0 = not true):

- vane wake interaction (3)
- mist carry over in third side load (3)
- end of curve operation (2).

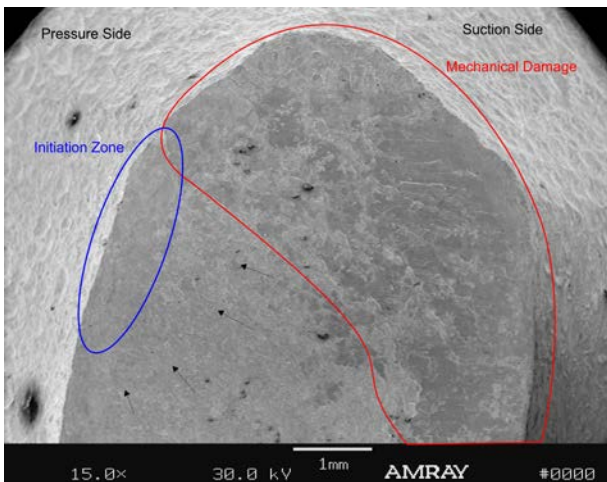The remaining sections of this paper discuss the verification work relating only to these three items.

Figure 9. SEM image showing the fracture surface at blade leading edge

It should be noted that a total of 117 actions were identified to prove or disprove the 12 hypotheses under HCF. Each action typically required some degree of analysis work to be performed by team members or third parties. The resulting planned scope of work and expenditure was enormous in comparison to most other RCFAs being performed by the End User. This was nevertheless, justified considering the potential massive loss in sales revenue caused by a forced LNG train outage if the propane compressor were to suffer major damage.

VANE WAKE BLADE INTERACTION

Impellers 3 and 4 each have 13 blades that discharge to a vaneless diffuser. They are downstream of a side load which has 14 guide vanes and a return channel with 16 vanes – see Figure 2. The separation distances are 21.3 and 9.5 inches (0.54 and 0.24 meters) between the third impeller inlet and its return channel vanes and side load vanes respectively. The corresponding distances for the fourth impeller are 18.9 and 10.3 inches (0.48 and 0.26 meters). The difference between the vane and impeller blade count is 3 and 1 for the return channel and side loads respectively. Based on classic analysis methods, as reported by (Kushner, 2004), only the impeller 1-diameter and 3-diameter disk modes could be excited under these conditions. Furthermore, the 1-diameter mode would only be excitable by the 14 guide vanes, and the 3-diameter mode would only be excitable by the 16 return channel vanes due to phase cancellation. The vane wake frequencies for the 14 guide vanes and 16 return channel vanes occur at 798 – 848 Hz and 912 – 970 Hz respectively. The frequency range is due to the permissible range of continuous shaft speed, 3420 – 3636 rpm. For blade leading edge modes there is no such phase requirement and they may be excited directly by the upstream wakes from return channel and side load vanes. Moreover, blade modal mistuning from variance in fabrication causes a natural frequency spread band which can make excitation of individual blades easier.

There are numerous references available in the open literature that discuss the detrimental effects upon impeller life from upstream wake interaction. For example, (Motriuk and Harvey, 1997) presented results from five large process gas compressors. The mechanism which causes distress to the impeller blading is associated with the pulsating dynamic force, applied as each low momentum wake is traversed during impeller rotation. This periodic forcing function may cause a resonant or non-resonant blade vibration resulting in a dynamic stress in the blades. The non-resonant response is normally tolerated as part of the design unless the wakes are able to become much stronger. This could happen during operation where excessive positive or negative vane incidence is encountered, for example during surge or choke. A resonant response may occur during allowable operation however, where vane wakes are encountered by the nearest impeller. This condition would not have been anticipated in the design.

Modal Analysis

In order to produce the impeller Campbell Diagrams it was necessary to determine the blade and disc modal frequencies. The method applied for this task was hammer impact testing as described by (Kushner, 2004). Tests were carried out on the third and fourth impellers from the 2007 and 2009 failed rotors. Hammer impacts were measured at fifteen locations near the leading edge of each of the 13 impeller blades. For measurement of the disc modes, the impeller was impacted on both the cover and hub side. There were a total of 104 impact locations on each side of the disk. For the cover side, there were a total of 52 impact locations on the blades (4 impact locations on each blade) and 52 impact locations on the cover (two concentric circles consisting of 26 points each).

Table 3 lists the fundamental blade leading edge mode frequency with the least amount of measured damping for both impellers. As previously mentioned, some mistuning is inevitable as a result of fabrication variance. The greatest being

a 12 percent difference from the average value for the failed 2007 fourth impeller. This was caused by the 13th blade 996 Hz measurement. One suspected reason for the low frequency measurement of the 13th blade is that the rupture of the two adjacent blades depressed this measured frequency. The CMM data for two blades of the fourth impeller and one blade of the third impeller showed consistent and in-tolerance manufacturing, which would tend to support this hypothesis. However, it is also possible that the modal frequencies of the ruptured blades were even lower which ultimately caused them to fail. The averaged value is plotted as a red line on Figures 10 and 11.

The testing also determined the 1-diameter cover/blades mode frequency for the fourth impeller to be 984 Hz. The margin above the highest 16X return vane frequency of 970 Hz is just 1.4 percent. Excitation of this mode could only occur if the expected diametral modes phase cancellation did not apply in this case. This was in fact, proven to be a remote, but possible scenario and is discussed later in the paper.

Third Impeller

Figure 10 is the Campbell diagram generated from the test measurements on the 2007 failed third impeller. The 14X and 16X vane wake frequencies, as well as twice these frequencies (28X and 32X) are plotted. Three excitable 3-diameter modes were found, one of the disk and two of the blades. The minimum percent separation margin for minor resonance is 11 percent below the 16X return channel vane wake frequency and 36 percent below 32X return channel vane wake frequency. Five 1-diameter modes were found, three of the disk, and two of the blades. The minimum separation margin for each of these excitable minor resonances is 19 percent above the 14X side load vane wake frequency and 19 percent below 28X side load vane wake frequency respectively. The 1-diameter disk mode is inherently difficult to excite due to shaft coupling.

The highest vane pass excitation from the 16X return channel vanes of 970 Hz is 7 percent below the lowest blade leading edge mode of 1040 Hz which is considered marginal. However, the blade with a long crack without a missing piece still had a blade frequency with margin from 16X speed. Although not plotted in Figure 10, the 17X and 18X signals would intersect the lowest blade mode frequency of 1040 Hz below the maximum continuous shaft speed. This was the main potential cause of blade resonance discovered from the testing. The side load with 14 vanes is a 90-degree inlet so that flow is non-uniform giving higher harmonics above 14X that could excite blade modes for the third and fourth impellers.

Fourth Impeller

Figure 11 is the Campbell diagram generated from the test measurements on the 2009 failed fourth impeller. The same vane wake frequencies, as for the third impeller are plotted. One 3-diameter mode was found of the disk. The percent separation margin for excitable minor resonance is 11 percent below the 16X return channel vane wake frequency. Three 1-diameter modes were found, two of the disk, and one of the blades. The minimum percent separation margin for each of these excitable minor resonances is 16 percent above the 14X side load vane wake frequency and 23 percent below 28X side

load vane wake frequency respectively. The 1-diameter disk mode is inherently difficult to excite due to shaft coupling.

Figure 12 shows the interference diagram based on FEA predictions for the fourth impeller. The left vertical axis represents the frequency in Hertz (Hz). The horizontal axis represents the nodal diameter mode shape of the impeller. The right vertical axis shows excitation harmonics of running speed. The blue diagonal lines represent maximum continuous speed times multiples or harmonics of running speed shown on the right vertical axis. The red vertical lines show potential excitation from the 14 side load guide vanes and the 16 return channel vanes upstream of the impeller. Lines are shown for both 1X and 2X excitation. Because the compressor can be operated over a variable speed range, the red lines are shown with an upper and lower limit represented by the bar at the top and bottom of the line. The upper limit is for 10 percent above maximum continuous speed and the lower limit is based on 10 percent below minimum continuous speed. The plus and minus 10 percent values are used to account for potential differences between predicted and actual natural frequencies. The inner bars represent actual continuous operating speed range from 3420 to 3636 rpm. The green diamonds represent calculated natural frequencies versus nodal diameter mode shape. The points labeled "0CxD" represent the fundamental impeller nodal diameter frequencies. Based on this data seven potential resonant points were identified and are labeled A through G.

The modal results indicate that there are no disk critical speeds of concern for both impellers. There are many impellers within the OEM's fleet that have interaction resonance of disk modes with upstream vanes, but this design does not.

Table 3. Blade natural frequency results from impact tests

	3rd Impeller			4th Impeller		
Failure	2009		2007	2009		2007
Blade	Damping %	Nat. Freq Hz		Damping %	Nat. Freq Hz	
#1	0.125	1088	1040	0.124	1121	missing piece
#2	0.133	1084	1072	0.157	1126	missing piece
#3	0.131	1084	1068	missing piece		1100
#4	0.132	1084	1068	0.163	1126	1100
#5	0.134	1046	1068	0.155	1126	1168
#6	0.131	1048	1068	0.139	1064	1108
#7	0.126	1084	1072	0.13	1121	1168
#8	0.130	1089	1072	0.127	1122	1192
#9	0.129	1088	1072	0.126	1122	1196
#10	0.124	1088	1068	0.124	1121	1192
#11	0.310	1089	1048	0.119	1121	1100
#12	0.144	1088	1064	0.121	1121	1072
#13	0.120	1088	1064	0.118	1121	996

In addition to the 9 impellers present on the End User's three propane compressors, the OEM has 17 other similar designed, full inducer impellers with 13 blades that immediately follow 14 vane side load inlets.

Steady State CFD Analysis

A steady state CFD analysis was performed on the fourth impeller to further investigate the vane wake interactions that were discussed previously. The model consisted of the entire 360 degree side load and return channel upstream of the impeller and a single representative rotating impeller vane passage, connected by a tangential control surface. The static

pressure was circumferentially averaged along this control surface but allowed to vary in the spanwise direction.
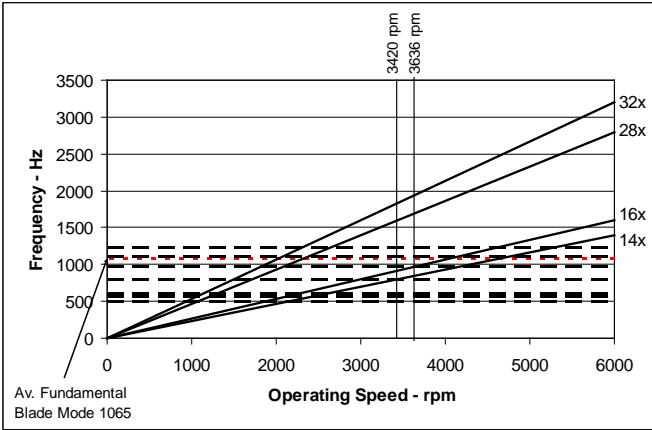

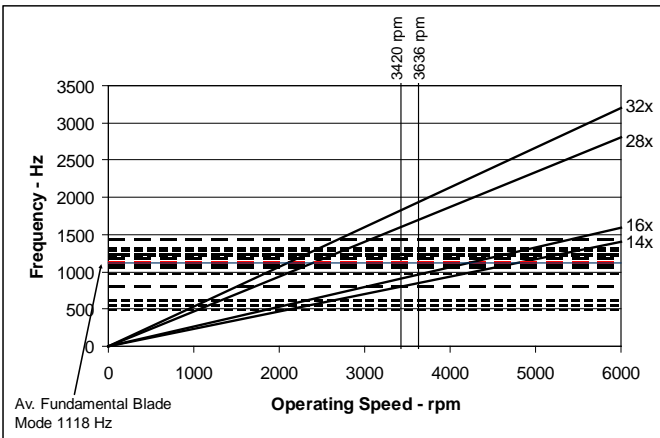*Figure 10. Third Impeller Campbell Diagram from 2007 failure*

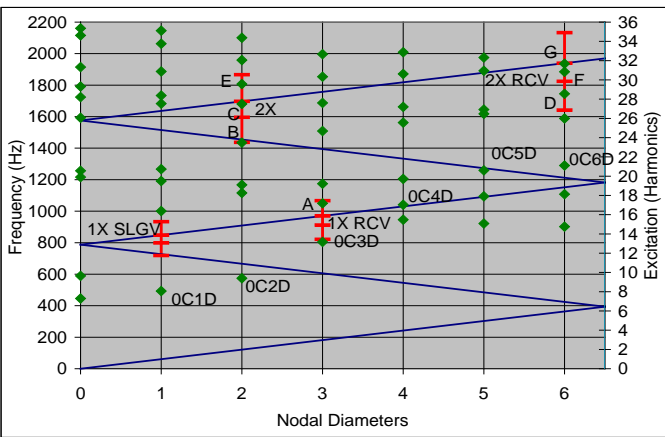*Figure 11. Fourth Impeller Campbell Diagram from 2009 failure*

Figure 12. Fourth Impeller Interference Diagram

Figure 13 shows the predicted pressure wake distributions for the 16X return channel vane and 14X side load vane wake frequencies. The applied operating boundary conditions were close to the compressor rated point although other cases close to surge and choke were also run. The results indicate that no large wakes in either domain are present and the maximum

pressure gradient is less than 2 psi (0.14 bar), which is about 2 percent of the fourth impeller inlet pressure.

A particular area of concern was how both 16X return channel and 14X side load wakes would interact at the impeller inlet. In order to assess this, the predicted static pressure distribution at the interface between the return channel and side load domains was analyzed using the Fast Fourier Transform (FFT) method. Results are shown in Figure 14 where no higher harmonics causing resonance were discovered. The mixing signal on the graph is the pressure at the interface between the return channel and side load flows. It is approximately equal to the sum of the pressure variations from the two individual streams.
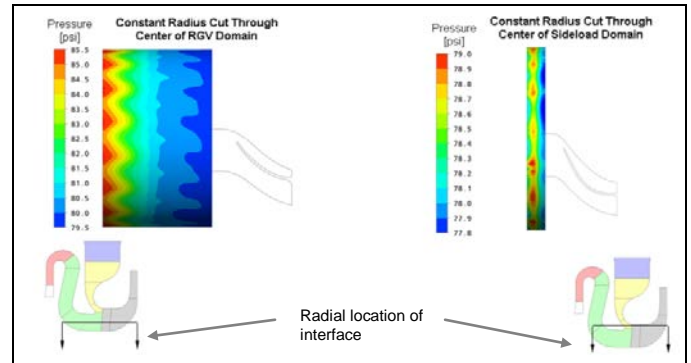

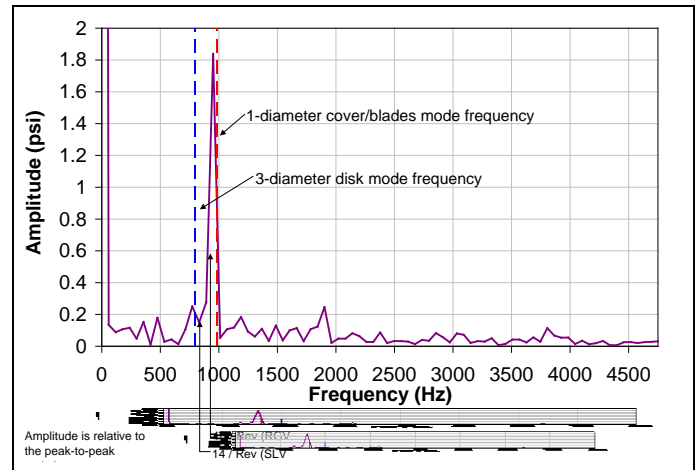*Figure 13. Fourth Impeller CFD results for vane wake impeller interface*

Figure 14. Fourth Impeller FFT for 16X and 14X combined signals

The measured 1-diameter cover/blades mode (984 Hz) is plotted as the red dashed line. This frequency is only slightly above the 16X return vane wake frequency and without phase cancellation would be considered resonant. A peak static pressure of just 1.8 psi (0.12 bar) was predicted and it was considered doubtful whether a significant alternating blade stress could result during resonance. For the 14X side load signal, the maximum peak to peak variation was only 3.2 psi (0.22 bar) during choke. Again, this was considered to be too low to be able to cause significant blade stress. The conclusion leading from the steady state CFD and FEA work was that the 16X, 14X and higher vane wake frequencies seemed unlikely to

cause resonant or non-resonant high blade stress.

On face value, there was little justification to further investigate vane wake interactions. Nevertheless, a decision was made to proceed with a full Fluid Structure Interaction (FSI) analysis because of the ability of gaining real insight to the unsteady and highly non-uniform flow regime at the impeller inlet. These conditions are created by the side load stream being along the outer periphery and having little mixing with the incoming return channel stream from the upstream impeller. Thus there is a different harmonic excitation at the side load area than for the return channel annulus.

Full Unsteady Fluid Structure Interaction Analysis of 1-Diameter Cover/Blades Mode

An FSI analysis consists of two main facets. The first being a full unsteady CFD analysis of the impeller and the second being a detailed dynamic structural FEA based upon the mapped dynamic pressure distribution from the CFD result. The advantage of following this approach is the ability to predict the dynamic blade stresses during a full impeller rotation. In contrast to the classic analysis methods, the full FSI analysis includes the complex simultaneous forcing function from both the side load stream and the return channel stream. As for steady-state CFD, this analysis assumed a dry gas condition; mist and transient liquid ingestion effects were not included.

The FSI analysis yields the maximum alternating stress on the blading. This is corrected for the effects of material and aerodynamic damping and plotted against the mean equivalent stress upon a Goodman Diagram. The mean equivalent stress is also corrected for the measured residual stress in the material. The fatigue endurance limit is found by plotting a straight line between the known alternating stress at failure with no applied mean stress and the ultimate tensile mean stress at failure with no applied alternating stress. If the point falls to the right hand side of this line, the endurance limit is exceeded and the blade would be susceptible to failure.

The CFD model included the return channel leading to the fourth impeller, the fourth impeller, the side load stream, side load nozzle, and the diffuser for the fourth impeller. It was meshed with 1.7 million elements and included the full 360 degree annulus. The computational model for the structural domain included the fourth impeller only since that is where the stresses of interest occur. It was meshed with 1 million elements. The predicted case was run at the rated volume flow and 3749 rpm, or 3 percent above the maximum shaft speed, in order to achieve excitation of the nearby 1-diameter cover/blades mode, previously discussed. 872 time steps were modeled which represents about 3.4 revolutions of the rotor. Only the last 256 time steps were used for the FFT to minimize the influence of start-up transient effects on the data.

Damping

Three primary forms of damping are cited for turbomachinery blades: material, mechanical, and aerodynamic. In the majority of cases, material damping of turbomachinery blades is comparatively small and therefore its contribution is often neglected. Mechanical damping can be significant in designs with root forms, covers, and other cases of frictional dissipation; however, such benefits are not available in blisk and impeller designs. This leaves aerodynamic damping as the primary source of damping for blisks and impellers. Aerodynamic damping accounts for vibratory energy dissipated due to the relative motion between the blade and the fluid. The main dependency parameters for aerodynamic damping are the fluid density, the blade mode shape during vibration, and the phase relation between the forcing function and the blade mode shape. The amount of damping is particularly important in determining alternating stress. While aerodynamic damping is known to be present, it is a somewhat controversial topic because its magnitude is difficult to determine. Furthermore, it varies based on the operation, and can even become negative in the case of flutter, which may be caused by flow separation. This is further complicated by the relatively few papers discussing impeller aerodynamic damping. Nevertheless, a proper assessment of the alternating stress cannot be made without an estimation of the damping, which is provided in the section on alternating stress.

Alternating Stress

The node showing the maximum response in the FEA was near to the weld toe, located at the leading edge cover. The predicted strain resulted in an alternating stress amplitude of 479 psi (3.3 MPa), assuming 10 percent modal damping. Scaling this value for the measured average material damping of 0.2 percent resulted in 23.9 ksi (164.8 MPa). Applying next, a known test-rig measured aerodynamic damping of 0.39 percent to this value resulted in a reduction to 12.3 ksi (84.8 MPa). The test rig measurement was taken from an open impeller with a 14.7 psi (101.4 MPa) inlet, (Lerche et al. 2010). Since the aerodynamic damping is approximately proportional to the inlet pressure (Kammerer and Abhari, 2009), a scaled value of 4.3 percent was obtained. This finally resulted in a corrected alternating stress of 1.1 ksi (7.6 MPa). The uncertainty of this value was however noted because of the origin of the applied aerodynamic damping being from an open impeller. A literature search was carried out by the OEM but no information was found for covered impellers. However, two particularly helpful papers by the same authors, (Kammerer and Abhari, 2009), were found for open impellers that quote aerodynamic damping values between 1 and 10 percent. They stated that aerodynamic damping measurements were consistently about 10 times greater than the material damping even at one bar inlet pressure. This would suggest that the most appropriate value for the present impeller would be near 2 percent rather than the applied 4.3 percent, leading to a greater alternating stress of approximately 2.4 ksi (16.6 MPa) under normal operation. It would also be reasonable to assume that damping would be lower for a covered impeller, since the amplitude of mode motion would be lower. However additional unknowns are as follows:

- literature results are with respect to air whereas the gas used was propane
- aerodynamic damping is heavily affected by operation and can either be reduced or become negative when operating either in or near choke. This could drive blades into flutter.

- mist carry over can affect aerodynamic damping as was shown by impeller flutter in case B-4 by (Kushner, 2004)

Mean Stress

The FEA indentified the maximum equivalent mean (von Mises) stress, due to impeller rotation, to be located at the leading edge cover weld fillet. A value of 179 ksi (1234.2 MPa) was predicted, see Figure 15. Since the yield strength is 90 ksi (758.4 MPa), this high local stress would result in local yielding. Therefore, 90 ksi was applied in the Goodman diagram for the mean stress. An elastic-plastic analysis would be needed to obtain a more accurate mean stress prediction.
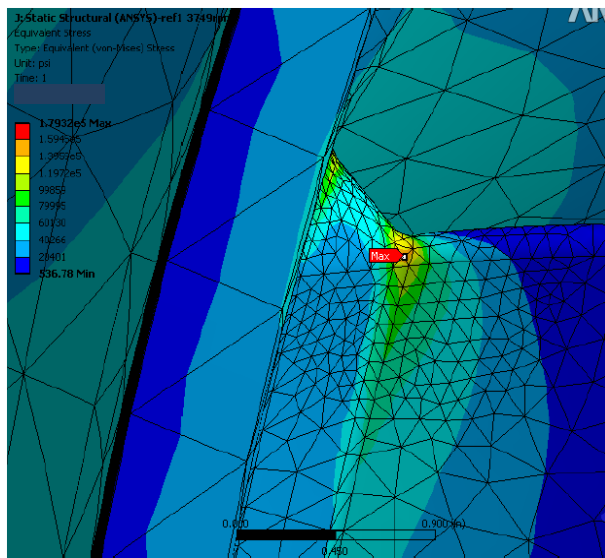

Figure 15. Fourth Impeller FEA result for maximum mean stress

Based on a step like feature on the fracture surface of one of the blades, it was suggested that residual tensile stresses may be present. The stress level in the impeller could be higher than expected if positive residual stresses are present. The OEM post weld heat treats impellers to reduce residual stresses, grinds the welds, and does over-speed tests, which locally yields the material and results in a compressive residual stress. In order to confirm the validity of this processing, residual stress measurements were made on both failed fourth impellers and one replacement impeller at the leading edge cover weld region. Two techniques were used to measure the residual stress. The first technique was the hole drilling method, where a strain gauge is used to determine the stress relieved by drilling a hole incrementally deeper into the material. Because this method is destructive and it was suggested that similar measurements be performed on a new impeller going into service, a second, non destructive technique was also employed. This second technique is called the nonlinear harmonics (NLH) method and was developed by a third party laboratory. This technique exploits the magnetoelastic effect, where the magnetic hysteresis and permeability, and accordingly, the harmonic content of the magnetic induction, are influenced by the stress state of the material (Kwun and Burkhardt, 1989). Blades 3, 7 and 12 were measured in each

impeller at carefully chosen locations on the suction surface. Results are shown in Table 4 where averaged values have been calculated from the individual measurements near the hub, cover and leading edge. The measured stresses were all compressive (negative sign) in nature, ranging between -14 and -21 ksi (-96.5 and -144.8 MPa). The conclusion drawn from these results was that residual stress could not have contributed to the early failure on the impeller blades. Furthermore, the compressive residual stress would have increased the allowable alternating stress. A conservative interpretation of the Table 4 results gives an appropriate value of -20 ksi (-137.9 MPa). This reduced the maximum mean equivalent stress found by FEA from 90.5 to 70.5 ksi (from 624 to 486.1 MPa).

Table 4. Fourth Impeller residual stress measurements

	First Failed Impeller	Second Failed Impeller	Replacement Impeller
	Average Minimum Principal Stress	Average Minimum Principal Stress	Average Minimum Principal Stress
Location	PSI	PSI	PSI
Hub	-20192	-18352	-13991
Shroud	-21080	-18304	-18775
Leading Edge	-19599	-18189	-17071

Goodman Stress Diagram

The Goodman diagram is able to assess the fatigue endurance of the impeller blade by integrating the limitations on alternating and mean stress to give a fatigue endurance limit line.

As previously discussed, the alternating stress limit is defined under the condition of zero mean equivalent stress. Due to the fact that the failures occurred at the toe of a weld and the properties in welds can be variable, it was difficult to determine what and if published fatigue data would be applicable. It was suggested that testing of the actual weldment would provide the most satisfying results. The testing consisted of T-sample fatigue testing of twelve samples taken from four individual blades of the 2007 failed fourth impeller. Each sample was taken across the weld region near the leading edge of the blade. The applied alternating stresses ranged from 95.1 ksi (655.4 MPa) to 39.6 ksi (273.2 MPa) and resulted in lives of 44 thousand cycles and 10 million cycles respectively. Failure was achieved at 73.7 ksi (508.1 MPa) stress and 965 thousand cycles for one sample but two other samples achieved run-out at 10 million cycles at slightly less stress, see Figure 16. The failure stress that was applied within Goodman diagram was taken in between these three points at 70 ksi (482.6 MPa). Despite the fact that the samples were taken from the actual failed impeller, which, in theory, would remove effects due to geometry and surface variations, the analysis included the assumption that the T-sample test did not represent the worst case. For example, it was observed that the surface at the leading edge had slightly more extensive damage due to erosion than the location the samples were taken from. Therefore, a reduction of the endurance stress was included to account for the effects of material surface flaws and deviation from averaged endurance results (reliability). These "K factors" were 0.7 and 0.81 respectively. The source for the values was taken from (ANSI/ASME B106.1M, 1985). The product of the K factors reduced the effective endurance limit for the

alternating stress to 39.7 ksi (273.7 MPa). It is noted that the use of these values is conservative. In particular, the K factor related to the surface is the value used if the sample tested had a mirror finish. The reliability K factor is essentially a statistical factor to account for the inherent variation in fatigue data. The value of 0.81 assumes that 99 percent of all samples tested at 70 ksi (482.6 MPa) do not fail after 10^6 cycles. This is a reasonable reduction given the number of samples available for testing.
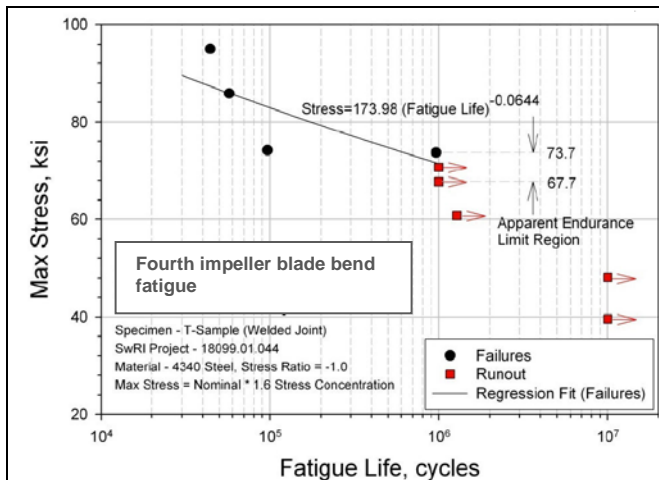

Figure 16. Fourth Impeller T-sample bend fatigue test results

The Goodman Diagram (Figure 17) has two individual plotted points. Two endurance limit lines are plotted; one with and one without the alternating stress K factors. Moving from right to left on the diagram; the first point represents conditions at 3636 rpm which is maximum continuous shaft speed. Applying the compressive residual mean stress of -20 ksi (-137.9 MPa) moves this point on to the second. This is located at a mean stress of 70 ksi (482.6 MPa) and the impeller endurance limit should be judged here. It indicates that a very high Goodman safety factor of 1.7 exists with an applied aerodynamic damping of 4.3 percent. The calculated alternating stress is only about four percent of the fatigue strength. If damping were to reduce to 0.16 percent it would exceed the lower endurance limit line and lead to probable blade failure. This value does seem low but is valid only under the assumption that no weld flaws were found at failure initiations, which could not be confirmed.

Due to the fact that the tensile test results on the fourth impeller from the 2007 failure were lower than specification, a concentration factor was also applied to the mean stress. However, the tensile properties of the other failed impellers were higher than required by the OEM's specification. This is again conservative in a failure analysis setting, particularly given that AISI 4340 is a ductile material.

Conversely, had the FSI analysis boundary conditions been applied closer to choke, the predicted exciting forces and resulting blade stress would be greater than shown in Figure 17. As will be explained later in the paper, this impeller is known to have run continuously in the vicinity of choke during the winter months.

In summary, the FSI prediction indicates that excitation of the 1-diameter cover/blades mode with the 16X return channel vane wake frequency results in significant but acceptable dynamic stress at the toe of the weld on the blade.
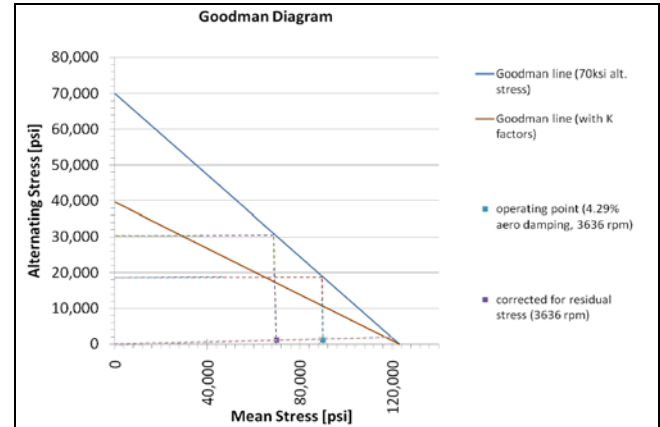

Figure 17. Fourth Impeller Goodman Diagram for 1-diameter cover/blades mode

This is contrary the conclusion drawn from the steady state CFD/FEA previously discussed and demonstrates the added value of performing the analysis. It implies that the diametral mode phase cancellation, previously assumed to prevent excitation from the 16X vane wake disturbance, was not entirely present. The most plausible reason for this unexpected result is that the non-symmetric grid for the FSI model causes the 1-diameter cover/blades mode to be slightly non-uniform which prevents complete phase cancellation. A physical contribution would also occur from any mistuning of the modal frequency caused by the welding procedure at the cover to blade interface.

If no aerodynamic damping is assumed, the stress would result in probable failure. Using typical values of aerodynamic damping published in the literature results in stresses lower than the endurance limit being predicted. However, the published data for aerodynamic damping is for open impellers that will likely have different characteristics than a covered impeller.

Since determining whether the blade endurance limit is exceeded or not heavily depends upon the aerodynamic damping, and the applied surface K factor previously discussed, it was impossible to reach an irrefutable conclusion. Nevertheless, the FSI analysis did identify significant stress at the blade weld toe and a low to medium confidence factor was attributed to the root cause with a grading of 2 (possibly true).

Mistuned Blade Leading Edge Mode Excitation

As is the case for the 1-diameter cover/blades mode, the leading edge mode frequencies of un-cracked blades were all tested and found to have margin from the 16X predominant forcing frequency. It is possible that the four total cracked blades actually had frequencies equal to 16X harmonic since no prior tests were done. The blade thickness of the single cracked third impeller blade however, was verified to be within specification. A crack could also initiate from a short transient after about an hour of running with a much higher harmonic containing (16 + 2)X from the side load flow. Propagation of a

crack under these circumstances would occur at a more gradual rate from lower forcing functions. For example, the highest flow analyzed with steady state CFD showed a harmonic excitation at 14 times speed (14X) to be as high as it was at 13 times speed (13X) at lower flow, one less than number of side load vanes. An increase and change in harmonic contact for compressor stages that are not uniform circumferentially are known to occur as flow approaches surge or choke, which would apply for inlets, side loads, and discharge stages (Sorokes, et al. 2006) and (Kushner, 2004).

Mistuning is known to increase response of some blades more in comparison to others. In addition to the many studies on axial flow machines, Hattori et al. (2008) is an example of a radial impeller where some blades responded much more than others. In some cases, mistuning can be the reason why one or a few blades have cracks due to fatigue as opposed to many blades. In this case the effect would be smaller as there are two disks supporting the blades, but the exact speed during an aggravating transient would also result in a large variation from blade to blade. For example, if the total damping is two percent, one blade could have twice the vibratory amplitude as another with a three percent change in speed. This percentage also corresponds to a similar difference between blade mode frequencies for the impellers tested.

Similar to the 1-diameter cover/blades mode, mistuning is a category of vane wake resonance. It was however, graded with a higher confidence factor; 3 (likely) based upon the evidence uncovered from steady state CFD at near choke conditions. Figure 18 shows how the 14X harmonic becomes stronger as choked conditions are approached. Other harmonics would undoubtedly become greatly amplified during deep choke so that total excitation over the entire spectrum, in addition to 13X and 16X, were the most likely sources for crack initiation.

The recommendations put forth to mitigate this root cause would be equally successful in preventing both possibilities of resonance identified above.
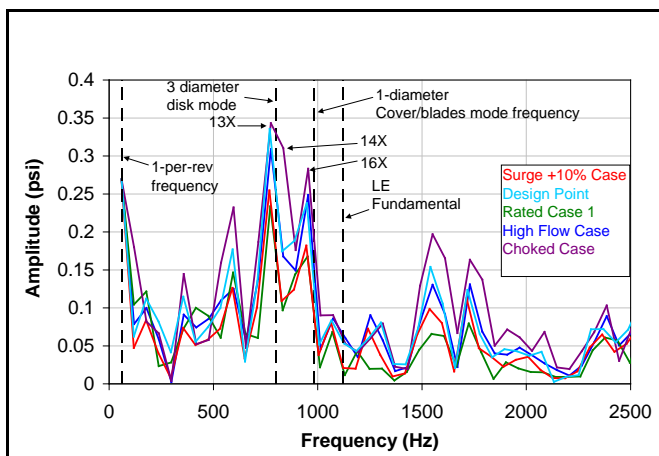

Figure 18. Fourth Impeller FFT plot of steady state CFD signals at impeller inlet

The strong 13X signal from the 14-vane side load is apparently caused by the nonuniform flow from the side entry. Flow entering from the side load nozzle is not turned completely to the radial direction by the vanes. This causes the strong wakes near the nozzle to fan out relative to the vane spacing, leading to lower harmonics. This effect was also observed by Higasio et al. (2010).

Mitigation Recommendations

Although the third impeller was not analysed by the FSI method, it was accepted that the failure root cause would also have been associated with a modal resonance. Based on the modal analysis results discussed previously, the most likely candidate would be the leading edge blade mode together with the (16+1)X or (16+2)X vane frequency. Accordingly, the required mitigation was to remove vane wake interaction resonances from both third and fourth impellers.

The RCFA team proposed two recommendations that can be regarded as separate items. The most important of these being a design modification of the existing impeller. The other being a redesign of the side load vanes and a reduction in their number from 14 to 7.

Impeller design modification

The major feature of the redesigned impeller was an increase in the radius of curvature at the failure location in order to affect the stress concentration. Since this could not be accomplished with the weld being located at the cover side, the weld was shifted to the hub side of the impeller. The blades will be integrally machined to the cover and welded to the hub. This results in the peak stress location being a machined contour with reduced stress concentration (factor of two or more smaller) and greatly reduced probability of any defect being present. Strain life calculations using stress concentrations based on the change of radius of curvature show that for a mean stress of 65 ksi (448.2 MPa), the alternating stress at 10^8 cycles is approximately 15 ksi (103.4 MPa) higher for the machined contour or for the same alternating stress, the lifetime is increased by four or more orders of magnitude (Figure 19). A further FSI study of the redesigned impeller showed a reduction in alternating stress by a factor of 7.1.

This is the design of the third, fourth, and fifth impellers on the rotor currently running in the compressor. To date, these impellers have over 15,300 hours of trouble free operation. Further modifications include the removal of the leading edge taper from the lower portion of the blade where it will be welded to the hub, a localized increase in the blade thickness where it is welded to the hub (similar to a "T" head design) and the hub and cover thicknesses have been increased. Shot peening will be performed on and around the weld to add further compressive residual stresses. The material composition will also be changed to 13Cr-4Ni, which offers benefits including better toughness, through hardenability and manufacturability over AISI 4340.

FEA results indicated that the separation margins from the vane wake sideload and return wake frequencies have been substantially increased (by approximately 10 percent) for all leading edge and hub to tip mode shapes.
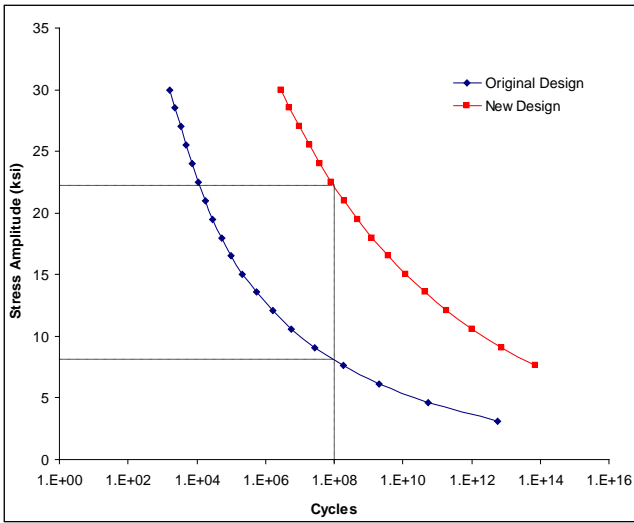
Figure 19. Plot of stress amplitude versus cycles for the original and modified designs

The interference diagram in Figure 20 shows even greater design margins compared to Figure 12, including the 1-diameter cover/blades mode that will be near 1100 Hz instead of 1000 Hz. In addition, changing the sideload inlet from 14 inlet guide vanes to 7 inlet guide vanes with spacing equivalent to 8 eliminates the 1 nodal diameter excitation potential. A potential resonance point is shown as point A.
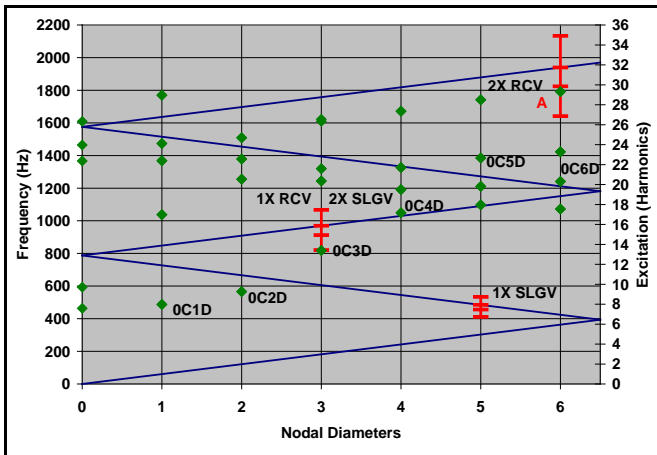

Figure 20. Fourth Impeller Interference Diagram change

This is a 6 nodal diameter pattern of the leading edge second mode at 1792 Hz. It would be resonant with 2 times the return channel vanes (32X) at 3360 RPM (slightly below minimum continuous speed). This mode would not be responsive as it is a second blade mode with a nodal line through the blade.

The equivalent stress at the leading edge cover radius was predicted now to be reduced to 59 ksi (406.8 MPa). Steady state CFD results for the individual fourth impeller stage showed similar performance characteristics to the original design.

Redesigned Side Load vanes

To eliminate the 14X signal from the side load and weaken the side load signal in general, a new side load vane design was proposed and analyzed. These highly curved vanes are spaced

at 8 per circle and are based on the OEM's current proven inlet design. This arrangement effectively removes the primary 14X wake frequency as shown in Figure 20. The predicted change in side load signal to the impeller at design point (DP) is shown in Figure 21. Harmonics would still of course be present but would cause a greatly reduced response, including the suspected main cause (16 + 2)X signal, if modal excitation were to occur. Although the vane cascade pitch is increased by a factor of two by the reduced number of vanes from 14 to 7, superior flow alignment into the vanes is achieved by introducing a tip curvature. Flow impingement onto the curved vane tip is more uniform and greatly reduces the formation of secondary flow. The advantage for the downstream impeller is a reduced vane wake, see Figure 22.
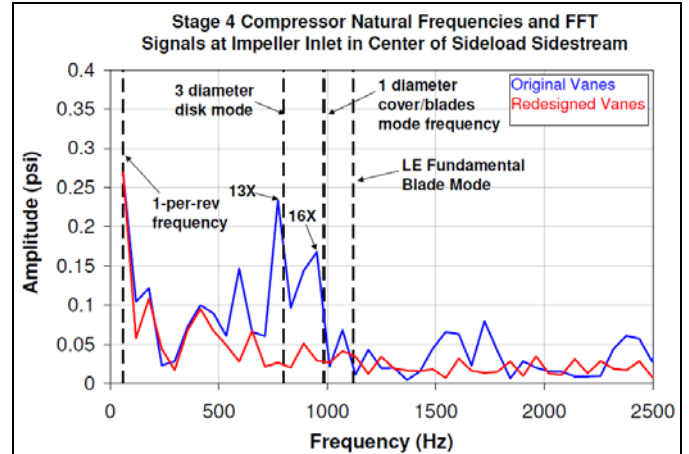

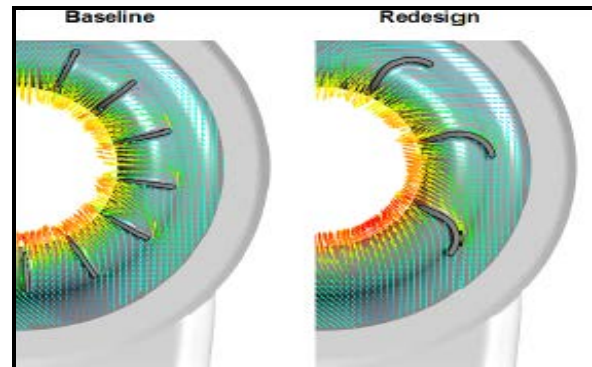Figure 21. Fourth Impeller FFT plot of steady state CFD Original and Redesigned side load signals

Figure 22. Side load vane CFD velocity profiles for Fourth Impeller

MIST CARRY OVER

The detrimental effects of liquid ingestion in refrigeration compressors have been well reported in the literature, for example (Kushner, 2000) and (Kushner, et al. 2000). One of the problems included ingestion from liquids upstream of anti-surge valves. If the liquid is in mist form, as expected in this case, the fluid density increases and results in a rise in head. Furthermore, the liquid evaporation creates additional gas volume which increases the downstream impeller flow velocity and pushes the rear stages towards or into choke. This situation is clearly made worse if the stages are already operating close

to choke. (Gresh, 2006) presented a case study for propylene refrigeration compressor with multiple impeller failures in the last section. It was proven that liquid carry over and choked flow were the root causes.

For refrigeration compressors, mist will be transferred to the suction scrubbers if complete evaporation has not taken place in the upstream heat exchanger. The amount of mist being transferred to the compressor is controlled by the scrubber mist eliminator pads. These pads coalesce the droplets by impingement so that liquid drains to the bottom of the drum under gravity. Mist eliminator pads are designed to remove droplets above a certain size for the specified range in suction flow rate. For smaller droplets the separation efficiency of the pads slowly reduces. If the suction flow rate exceeds the maximum handling capacity, the separation efficiency drops rapidly. This is termed "overload" and the large droplets that have formed in the mesh are no longer able to drain to the bottom of the drum. Instead they become re-entrained with the gas leaving the pads and are carried over into the compressor.

(Kushner, et al. 2000) discussed how vane wakes can be aggravated when liquids are present. Their results discussed impeller damage in four identical refrigeration compressors. The failure cause was attributed to interaction resonance accompanied with liquid ingestion. Besides aggravating vane wakes, liquid would also increase non-uniform loading from the side load due to the 90 degree inlet configuration shown in Figure 2. This would also aggravate wakes and increase the likelihood of impeller mode excitation.

Evidence that liquid ingestion may have occurred was presented during the RCFA performed after the first failure. Figure 23 shows a horizontal stain on a diaphragm taken from the compressor. Swirl patterns (Figure 24) were found on all of the impellers. Erosion damage was found on the pressure side of both the third and fourth impeller blades. This possible cause was a point of contention, but was not pursued further since it was believed that sufficient precautionary measures were in place and the erosion damage was caused by the large amounts of solid deposits which were also found in the gas paths of the impellers. Because it was left as an unclosed item, it was revisited in more detail during the current RCFA.

Figure 23. Photograph showing stains on a diaphragm

Side load Mist Eliminator Pad Overload

A review of continuous historical operating data between February 2006 and December 2009 was carried out for each of the four scrubbers shown in Figure 1. This was done for all three LNG trains. Each scrubber is fitted with the same heavy duty, high efficiency horizontal mist eliminator design. Only the diameter varies from vessel to vessel to accommodate the differences in volumetric flow rate. In each case, the maximum Souders-Brown K-factor (Souders, and Brown 1934) was restricted to 0.105. Values above this limit would imply a reduction of drainage from the mesh pad resulting in possible mist carry over into the downstream compressor stage.

Figure 24. Photograph of the 2007 failed rotor showing swirl patterns on the impellers.

The analysis confirmed that the first and third side load scrubber mist eliminators had consistently exceeded their limits. Focus was however, given to the third side load because it was the worst case and is located immediately upstream of the fourth impeller. The results are plotted in Figure 25 for Trains 3, 4 & 5. The horizontal dashed line denotes the maximum limit. The plotted points were selected with the greatest measured flow rates to show the general trend throughout the year. A clear periodic swing is shown for each train as the volumetric flow rate varies between high during summer and low during winter. This is caused by the increased refrigeration duty as a result of the higher sea water cooling temperature in the hotter months. During the summer, Trains 3 and 4 exceeded the K-factor limit by as much as 10 percent. Train 4 was marginally worse in the latter two years. Data for Train 5, which began operating in early 2006, was unavailable before February 2008. This train only exceeded the limit by 2 percent in 2009.

Erosion Analysis

As part of the metallurgical analysis, the surface and cross section of samples taken from the 2007 and 2009 failed fourth impellers were examined using optical and electron microscopy. The location of the samples was just above the cover weld dressing marks at the leading edge. This region was close to the earlier identified high stress region and crack inception site. In both cases surface erosion was discovered on the pressure side of the sample. Figures 26 and 27 show the cross sectional images of each side of the blade on the left and the corresponding surface image on the right.
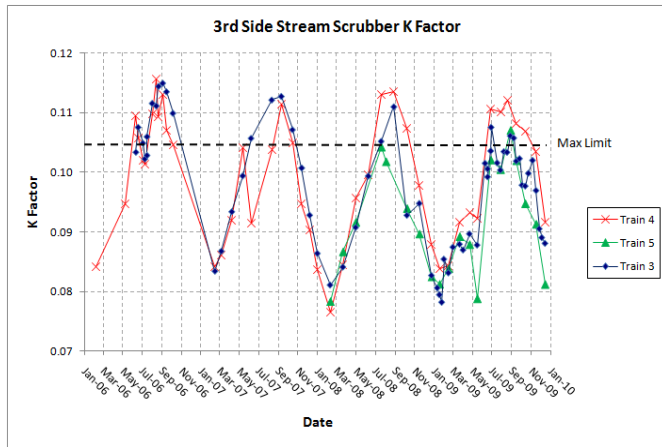
Figure 25. K factor for Trains 3, 4 & 5 - third side load

Comparing the cross sectional images in both figures, it is evident that the pressure side of the blade is irregular, while the suction side is essentially flat. As expected, the same observation can be made by comparing the surface images. The suction side surfaces still show the machining marks from the manufacturing of the impellers.
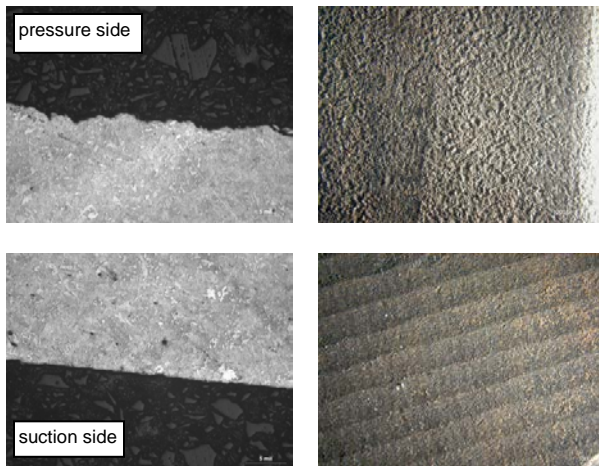

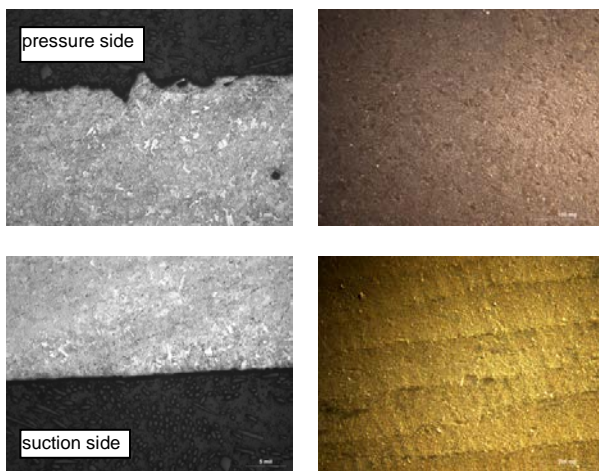*Figure 26. Images of 2007 Fourth Impeller released piece*

Figure 27. Images of 2009 Fourth Impeller released piece

These marks are no longer visible on the pressure side surfaces. It is very clear that the pressure side of the blades were subject to erosion by some media. Closer examination of the morphology of the surface shows that the erosion damage can be attributed to liquid droplet impingement.

In summary, strong evidence was uncovered to support the hypothesis for liquid carry over in the form of mist in the third side load. It is likely that the mist would have contained droplets well above the design intent of 10 microns diameter. The amount of liquid is unknown because direct measurement was impossible due to the inlet piping orientation. The OEM recommended maximum was 1 percent by weight for droplets no larger than 0.4 mils (10 microns) diameter. This limitation was however, imposed only to avoid liquid erosion.

The fourth impeller had at least one ruptured blade in both 2007 and 2009 failures which tends to support the notion of greater (aggravated) wakes being present. On the other hand, it is not known how the upstream third impeller, which had a single cracked blade in 2007, would have been affected by liquid induced wake resonance from the downstream third side load. Accordingly, this root cause hypothesis was graded with a medium confidence factor of 3 (likely).

Mitigation Recommendations

The objective was to remove the possibility of mist carry over from the third side load scrubber. The obvious solution was to upgrade the mist eliminator to handle the required amount volumetric flow rate during the summer months. Consultation with the vessel OEM confirmed that a replacement would be possible to accommodate an extra 19 percent of flow. Considering the results in Figure 25, this would still leave a positive margin of approximately 10 percent. Site work could be easily incorporated within the next available scheduled train shutdown. It was decided to apply the same upgrade to Trains 3, 4 & 5.

It was also recommended to upgrade the first side load scrubber mist eliminator to obtain a similar increase in maximum flow rate.

END OF CURVE OPERATION

This section discusses the third and final root cause hypothesis that was proven to have some degree of validity. As the title suggests, it applies to operation of the relevant compressor section in the end region of the OEM's compressor curve. As will be discussed later, there was some uncertainty associated with the predicted operating points and whether choked flow had actually occurred. Nevertheless, it was clear that continuous operation had occurred for months at very high flow rates for the fourth compressor section.

For LNG production, the refrigeration compressors typically handle high volumetric flow rates because of the economy of scale. As such, the impeller flow coefficient even in the rear stages is usually larger than 0.12. As discussed by (Sorokes, et al. 2006), these types of impellers have tall blade leading edges making them prone to flex or flutter if subjected to sufficiently high dynamic force. Moreover, the leading edge is the thinnest part of the blade which makes it more susceptible to fracture. High impeller meridional velocities in choke may cause greater circumferential flow distortion at the exit of the upstream vanes. This leads to wakes with larger static pressure differentials across them and causes a greater dynamic force on

the impeller blades and possible failure.

(Sorokes, et al. 2006) gave a relevant example where a compressor processing a heavy hydrocarbon gas had impeller blade fractures caused by operation in choke. The impeller in question was a high flow coefficient design. Furthermore, it was a covered two piece impeller, welded at either the hub or cover. Blade failure was encountered at the leading edge with a continuous fracture extending from the hub to tip. This case has remarkable similarities to the one reported herein, considering the type of compressor service, impeller design and blade failure.

High flow rates approaching choke for compressor sections with volutes or side load sections are known to have greater non-uniform forces as blades rotate through the flow field. In this case the side load non-uniformity is an area to improve for added reliability. Vaned diffusers to minimize leading edge mode excitation when in the choke regime are not an option due to lower flow capability.

Field Data Analysis

65 data points were chosen from the performance monitoring database for Train 3. One point per week was chosen for the duration between the first and second failure shutdowns in June 2007 and May 2009. The criterion used to select each point was the highest measured mass flow rate at the discharge venturi meter. The performance of each compressor section was predicted using four different software packages, three of which were proprietary. The commercially available software package (Flexware) uses measured inlet pressure and temperature, gas properties, mass flows and shaft speed for each inlet. Thermodynamic calculations between two state points are done by applying the Redlich-Kwong equation of state. The main challenge associated with this approach is that the discharge temperature of each compressor section is not measured and can only be estimated by assuming a polytropic efficiency. The first section discharge flow combines internally with the known pressure, temperature, and mass flow of the first side load to form the inlet conditions for the second section. This is repeated for each section so that any inaccuracies can compound up to the fourth and final section. If the calculated fourth section discharge temperature does not match what is measured, the program logic will adjust work in all sections by an equal amount until the final temperatures match. Work is defined as polytropic head divided by polytropic efficiency. This has the effect of altering section polytropic efficiency and calculated discharge temperature. Although measured properties were typically well matched, some uncertainty still remained about the inlet conditions of the second, third and fourth sections. Another source of potential error came from the mass flow into the fourth section. Flow from the third side load is not a measured value, rather it is calculated from the final discharge flow minus the main inlet, first side load and second side load flows. Therefore, if any of these flows are in error, this error will also affect the mass flow calculated into the fourth section.

The results are plotted in Figure 28 in the form of head coefficient versus flow coefficient for the fourth section. The rated performance curve determined by the OEM factory acceptance test is also included for comparison. In general the points match the curve well although there is a larger scatter towards the end of curve. The winter points were located at the highest flow rates because of the greater gas turbine power available during that time of year. Based on the Flexware prediction, none of the points were found to be located beyond the end of the curve (in choke) however, four points during December 2007 were in the end of curve region as indicated by a ring in the plot.
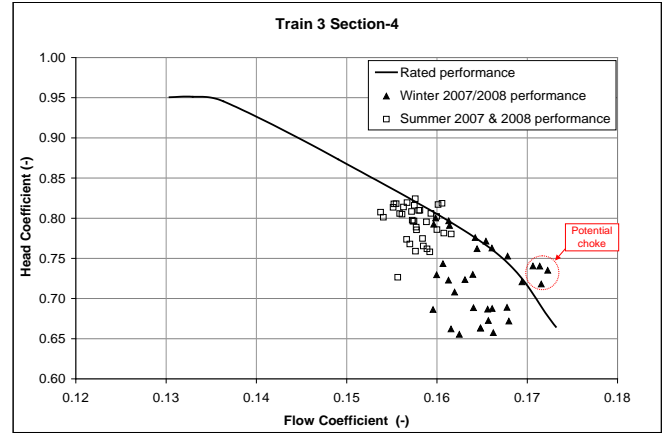

Figure 28. Fourth Section head versus flow coefficient – Train 3

In reality an error band of at least 3 percent is applicable to all the points shown, based on the calculation and measurement uncertainties discussed above. It is possible that the four marked points could have been operating in choke. Furthermore, the other programs indicated up to twelve points near the end of curve region with some points potentially in choke, or certainly in choke if considering a 3 percent uncertainty. Another observation is that the weekly flow trends, from which each point was selected, did not tend to fluctuate a great deal. This confirms that these adverse operating conditions would have persisted for hours or even days.

In summary, the analysis of 65 operating points between the first and second impeller failures identified the fourth compressor section to have been operating very close to choke. The same conclusion was made for the first section although focus remained on the fourth section due to the failed fourth impeller. Sections two and three were satisfactory with flow coefficients nearer to their mid curve regions. Depending on the method of analysis, four to twelve out of the 65 data points were found to be located at the end of the OEM curve and potentially in choke. As a result of the uncertainty surrounding the prediction of the internal volumetric flow rates and limited number of analysis points, a definitive conclusion could not be made. Accordingly, this root cause hypothesis was graded with a low to medium confidence factor of 2 (possibly true).

Mitigation Recommendations

Two recommendations were made in order to avoid the possibility of operating in choke in the future. The first was to introduce a choke margin alarm in the distributed control system so that the operator would be warned not to push the compressor string capacity beyond this point. Only a 1 percent

margin could be justified when balanced against the corresponding loss of refrigeration duty.

The second recommendation was intended as the long term solution. A re-wheel study has recently begun with the OEM for all five impellers and their static flow path components. This would relocate the current operating points further to the left in Figure 27. Not only would this provide more margin from choke but it would also lead to a greater overall efficiency.

TRAIN CHANGE ANALYSIS

Searching for a reason why Trains 4 and 5 had not failed in a similar manner to Train 3, which had failed twice, required a change analysis to be performed. This was basically a comparison between the three trains for a plethora of different parameters. One group consisted of monitored performance indicators, including bearing vibrations and thrust loads. A second group considered the compressor hardware including the isometrics leading up to each flange. Fabrication methods and material specifications were also scrutinized. No significant differences were uncovered by the analysis. As such, the investigation concluded that Trains 4 and 5 were very likely to encounter the same failures at some time in the near future.

In fact, this conclusion was verified in September 2010 when, the Train 4 compressor suffered a large step change in 1X vibration at both journal bearings during steady state operation. The greatest step being at the drive end bearing with a peak amplitude of 5.1 mils (130 microns). Based upon the previous two occurrences on Train 3, it is very likely that the third and/or fourth impeller failure(s) has occurred again. Confirmation will be possible upon inspection during the scheduled shutdown in May 2011.

CONCLUSIONS

Three root causes were positively identified from the investigation with varying degrees of confidence, commensurate with the supporting evidence for each one. However, it is apparent that they are not likely to be independent from one another. The most probable resonant frequency mode was identified as a severely mistuned leading edge mode for the fourth impeller. It is likely that mist carry over or choked operation (or both) also contributed to the excitation through the aggravation of upstream vane wakes. A combination of the above factors as a transient is also plausible since less than two hours of response near 1000 Hz is needed for crack initiation.

The investigation did not consider the third impeller failure in as much detail as the fourth impeller. As such, there remains some uncertainty about the failure mode. It is unknown whether this impeller experienced very short spells of choked operation during transient operation. The effect of a choked downstream fourth section on the third impeller is as well unknown without considerable analysis. Likewise, the effect of two ruptured blades in the fourth impeller on the third section aerodynamics is also unknown. The available evidence does indicate an intersection of the (16+2)X excitation frequency with the lowest blade mode frequency of 1040 Hz below the maximum continuous shaft speed. The facts tend to suggest that resonance may have occurred under normal operating conditions which is

cause for concern. It cannot, on the other hand, be ruled out that this section also may have encountered mist carry over for short periods of time as a result of the fourth impeller failure. Therefore, the same three root causes remain for the third impeller consisting of resonant frequency mode, mist carry over and choked operation.

The mitigation items that were proposed by the team have been approved by the End User's senior management. Their implementation will be expedited because the impeller failure detected in October 2008 occurred after only 11,000 total operating hours. At time of publication Train 3 has surpassed 15,300 total operating hours and will be required to run until the next scheduled outage on 13th May at 16,000 hours. Train 4 is being closely monitored and is planned to operate until the next scheduled shutdown on 16th May 2011.

NOMENCLATURE

APCI	=	Air Products and Chemicals Incorporated
bar	=	Bar (100,000 Pa)
CFD	=	Computational Fluid Dynamics
CW	=	Sea Cooling Water
C1X	=	Compressor Driver End X probe position
C1Y	=	Compressor Driver End Y probe position
C2X	=	Compressor Non Driver End X probe position
C2Y	=	Compressor Non Driver End Y probe position
C3	=	Propane
CMM	=	Coordinate Measuring Machine
Cr	=	Chromium
D	=	Impeller exit diameter
DP	=	Design Point
FEA	=	Finite Element Analysis
Flow Coefficient	=	$700Q/ND^3$
FSI	=	Fluid Structure Interaction
FFT	=	Fast Fourier Transform
g	=	Gravitational Acceleration
HCF	=	High Cycle Fatigue
H	=	Polytropic Head
Head Coefficient	=	H/U^2g
HP	=	High Pressure
K	=	Stress Concentration Factor
K-factor	=	Souders-Brown Factor $v/[(\rho_l - \rho_g)/\rho_g]^{1/2}$
ksi	=	Kilo Pounds per Square Inch
LNG	=	Liquefied Natural Gas
LLP	=	Low Low Pressure
LP	=	Low Pressure
MCHE	=	Main Cryogenic Heat Exchanger
mils	=	Thousandths of an Inch
MP	=	Medium Pressure
MPa	=	Mega Pascal
MMscfd	=	Million Standard Cubic Feet per Day
MR	=	Mixed Refrigerant

MMscmd	=	Million Standard Cubic Meters per Day
Mtpa	=	Million Tonnes per Annum
N	=	Compressor Shaft Speed
NGL	=	Natural Gas Liquid
Ni	=	Nickel
NLH	=	Non Linear Harmonics Method
psi	=	Pounds per Square Inch
Q	=	Volumetric Flow Rate
RCFA	=	Root Cause Failure Analysis
RCV	=	Return Channel Vane
SEM	=	Scanning Electron Microscope
SLGV	=	Side Load Guide Vane
U	=	Tangential Velocity at Impeller Exit
v	=	Maximum allowable gas velocity
ρ_g, ρ_l	=	Gas, Liquid density

APPENDIX A –
Final Status of RCFA Logic Tree
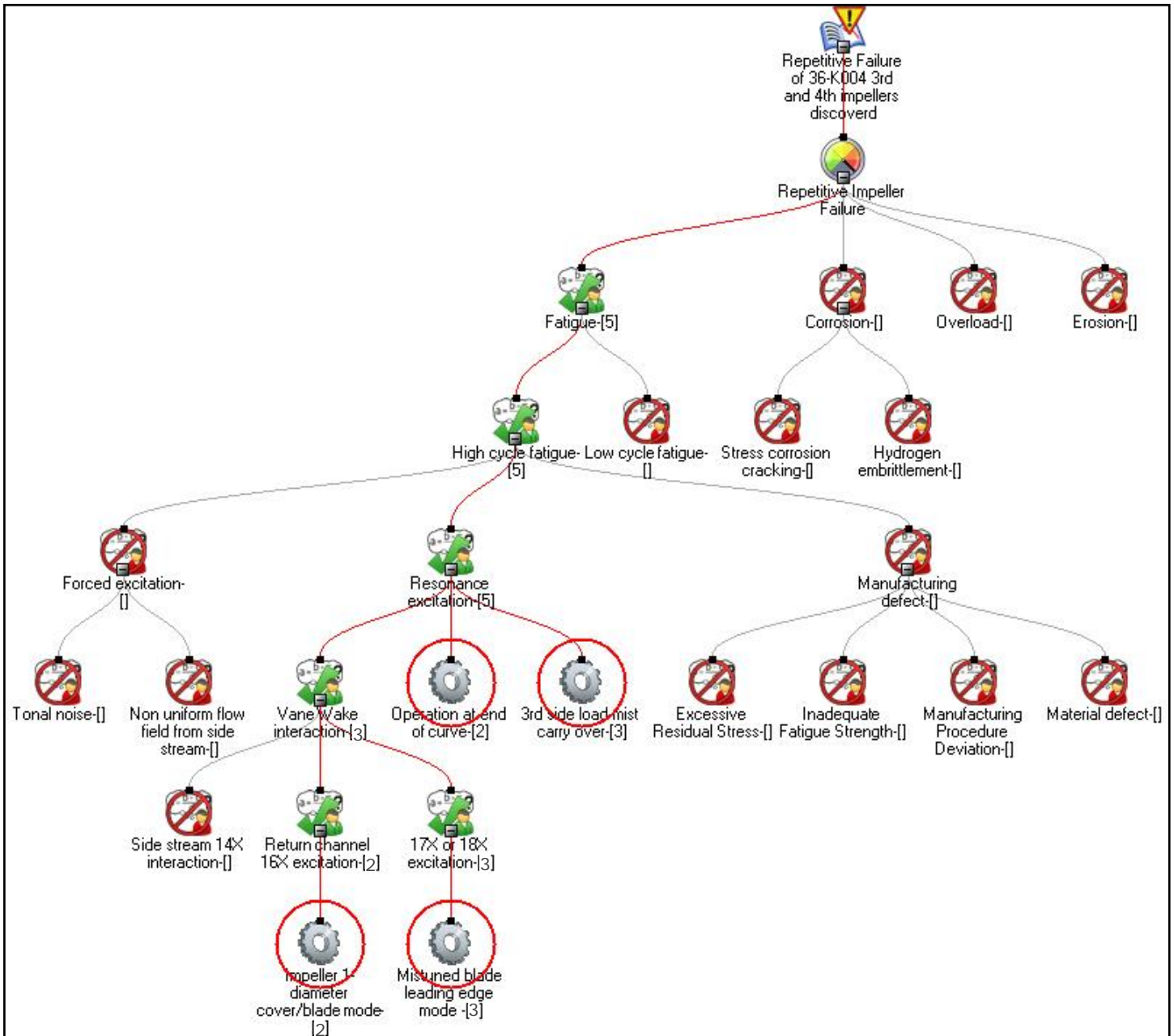
REFERENCES

ANSI/ASME B106.1M, "Design of Transmission Shafting", The American Society of Mechanical Engineers, 1985.

Gresh, T. "Avoid Refrigeration Compressor Damage". Article in Hydrocarbon Processing, Gulf Publishing Company, Pages 93-94, October 2006 Issue.

Hattori, H., Unno, M., Hayashi, M., "Mistuned Vibration Of Radial Infow Turbine Impeller", Journal of Fluid Science and Technology, Vol 3, No. 6, 2008, pp 764-774.

Higasio Atsushi, Yamashita Hiroyki, Ota Mitsuhiko; "Dynamic Stress Measurement of Centrifugal Compressor Impeller and Study for Strength Criteria Based On Correlation By Unsteady CFD," Proceedings of the Thirty-Ninth Turbomachinery Symposium, Turbomachinery Laboratory Texas A&M University System, 2010, pp. 43-48.

Kammerer, M. and Abhari, R. "Experimental Study on Impeller Blade Vibration During Resonance Part2: Blade Damping". Journal. Engineering. Gas Turbines Power, Volume 131, Issue 2, March 2009.

Kammerer, M. and Abhari, R. "Experimental Study on Impeller Blade Vibration During Resonance Part1: Blade Vibration Due to Inlet Flow Distortion". Journal. Engineering. Gas Turbines Power, Volume 131, Issue 2, March 2009.

Kushner, F. "Compressor Blade and Impeller Rotating Disk Vibration Avoidance Parameters", Proceeds of the ASME Conference for Challenges and Goals for Pipeline Compressors, Orlando, Fl, PID-Vol 5, November 2000.

Kushner, F., Richard, S. and Strickland, R. A. "Critical Review of Compressor Impeller Vibration Parameters For Failure Prevention", Proceedings of the 29th Turbomachinery Symposium, Turbomachinery Laboratory, Texas A&M University, College Station, 2000.

Kushner, F. "Rotating Component Modal Analysis And Resonance Avoidance Recommendations", Tutorial, Proceedings of the 33rd Turbomachinery Symposium, Turbomachinery Laboratory, Texas A&M University, College Station, TX. pp. 143-161, 2004.

Kwun, H. and Burkhardt, G.L. "Electromagnetic Techniques for Residual Stress Measurements", Metals Handbook Ninth Edition Volume 17: Nondestructive Evaluation and Quality Control, ASM International, Materials Park, OH, 159-163, 1989.

Lerche, A., Moore, J. J. and Yusheng, F. "Computational Modeling and Validation Testing of Dynamic Blade Stresses in a Rotating Centrifugal Compressor using a Time Domain Coupled Fluid-Structure Computational Model", Proceedings of ASME Turbo Expo 2010: Power for Land, Sea and Air, GT2010, Glasgow, UK, June 14 – 18, 2010.

Motriuk, R. W. and Harvey, D.G. "Root cause investigation of the centrifugal compressor pulsation/vibration problems". ASME, AD, v53-2, 4th International Symposium on Fluid-Structure Interactions, Aeroelasticity, Flow-Induced Vibration and Noise. 1997.

Sorokes, J. M., Miller, H. F. and Koch, J. M. "The Consequences of Compressor Operation in Overload", Proceedings of the 35th Turbomachinery Symposium, Turbomachinery Laboratory, Texas A&M University, College Station, 2006

Souders, M. and Brown, G. G. "Design of Fractionating Columns, Entrainment and Capacity" Industrial & Engineering Chemistry Journal, volume 38, issue 1, 1934.

Roberts M.J., Bronfenbrenner J.C., Yu-Nan L. and Petrowski J.M. "Increased Capacity Single Train AP-X[TM] Hybrid LNG Process". GASTECH Conference, October 2002, Doha.

ACKNOWLEDGEMENTS